


Employing Lewis Acidity to Generate Bimetallic Lanthanide Complexes

Bonnie E. Klamm,[‡] Thomas E. Albrecht-Schmitt, Ryan E. Baumbach, Brennan S. Billow,[‡] Frankie D. White, Stosh A. Kozimor, Brian L. Scott, and Aaron M. Tondreau*

 Cite This: *Inorg. Chem.* 2020, 59, 8642–8646

 Read Online

ACCESS |

 Metrics & More

 Article Recommendations

 Supporting Information

ABSTRACT: With the advent of lanthanide-based technologies, there is a clear need to advance the fundamental understanding of 4f-element chelation chemistry. Herein, we contribute to a growing body of lanthanide chelation chemistry and report the synthesis of bimetallic 4f-element complexes within an imine/hemiacetalate framework, $\text{Ln}_2\text{TPT}^{\text{OMe}}$ [Ln = lanthanide; TPT^{OMe} = tris(pyridineimine)(Tren)tris(methoxyhemiacetalate); Tren = tris(2-aminoethylamine)]. These products are generated from hydrolysis and methanolysis of the cage ligand tris(pyridinediimine)bis(Tren) (TPT; Tadanobu et al. *Chem. Lett.* 1993, 22 (5), 859–862) likely facilitated by inductive effects stemming from the Lewis acidic lanthanide cations. These complexes are interesting because they result from imine cleavage to generate two metal binding sites: one pocketed site within the macrocycle and the other terminal site capping a hemiacetalate moiety. A clear demarcation in reactivity is observed between samarium and europium, where the lighter and larger lanthanides generate a mixture of products, $\text{Ln}_2\text{TPT}^{\text{OMe}}$ and LnTPT . Meanwhile, the heavier and smaller lanthanides generate exclusively bimetallic $\text{Ln}_2\text{TPT}^{\text{OMe}}$. The cleavage reactivity to form $\text{Ln}_2\text{TPT}^{\text{OMe}}$ was extended beyond methanol to include other primary alcohols.

The selective complexation of lanthanide ions in coordination chemistry is important for many different areas, including the design of metal complexes for diagnostic and imaging^{2,3} applications, therapeutic agents,^{4,5} and the preparation of selective metal extractants for hydrometallurgy⁶ and nuclear waste management.^{7–10} However, the selective complexation of Ln^{3+} cations is challenging because of their similar physical and chemical properties. According to the classification by Pearson,¹¹ they behave as hard Lewis acids of similar radii with contraction of the ionic radius from La^{3+} to Lu^{3+} by 16%. The decrease in size substantially influences the lanthanide reactivity, such that the behavior of early lanthanides often differs from that of late lanthanides.^{12–14}

Developing chelating ligands for selective lanthanide coordination continues to be an important area of research. Ligands with appropriate binding sites have been designed to form a variety of lanthanide cryptates and received substantial interest as multidentate ligands with unique topological properties and as chelates for bimetallic systems.¹⁵ Cryptands have previously been generated via template synthesis using lanthanide metals as catalysts to assist with the formation of imine bonds, using the inherent Lewis acidity of lanthanide metals to template the formation of macrocycle compounds in situ.^{16–18} Here, we invert this paradigm and exploit the lanthanide Lewis acidity to achieve imine-cleavage reactions that generate bimetallic f-element complexes with imine-based cryptand ligands. The cleaved cage retains an (imino)pyridine coordination site that envelops the Ln^{3+} cation. A hemiacetalate functionality is also formed, which caps the macrocycle with a second Ln^{3+} ion. Hemiacetalate coordination remains rare in lanthanide chemistry, where only a handful

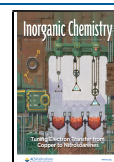
of similar complexes have been reported with lanthanide metals.^{19–21}

The synthesis of cryptand tris(pyridinediimine)bis(Tren) (TPT) was previously described by the condensation of 2,6-diformylpyridine with tris(2-aminoethyl)amine (Tren).¹ These previous efforts described syntheses using TPT and lanthanide cations with either aprotic acetonitrile, protic methanol (MeOH), or a mixture of both solvents. Those reactions were also heated at reflux to generate encapsulated lanthanide complexes. Several TPT lanthanide cryptates were synthesized by this method, forming the reported encapsulated metal complexes LnTPT (Ln = Nd, Eu–Tb) as red blocklike crystals that were sparsely characterized because of poor solubility (Scheme 1a).^{22–25}

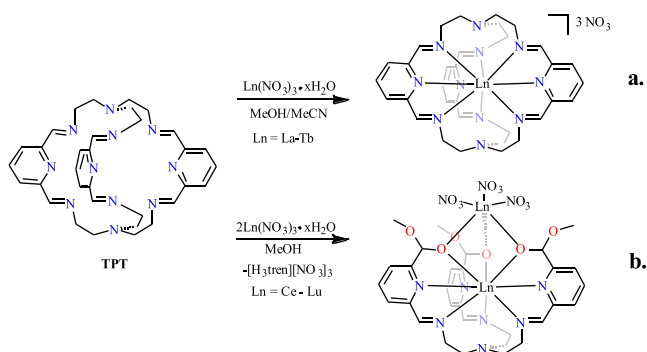
In this study, a divergence of the TPT coordination activity of the lanthanides is shown, where both mono- and bimetallic complexes that arise from cleavage of the ligand were generated (Scheme 1). These compounds were prepared by the addition of TPT to $\text{Ln}(\text{NO}_3)_3$ in MeOH at room temperature, generating either orange or yellow solutions. Crystals formed overnight from MeOH, and the solid-state structures were investigated by single-crystal X-ray diffraction. These studies revealed that imine cleavage occurred to generate the bimetallic $\text{Ln}_2\text{TPT}^{\text{OMe}}$ [Ln = lanthanide; TPT^{OMe}

Received: March 19, 2020

Published: June 17, 2020



Scheme 1. Summary of the Synthesis of (a) the Prior Synthesis of Ln₂TPT and (b) This Work's Synthesis of Ln₂TPT^{OMe}



= tris(pyridineimine)(Tren)tris(methoxyhemiacetate); Tren = tris(2-aminoethylamine)].

Ce₂TPT^{OMe} and Pr₂TPT^{OMe} were isolated as orange blocks and yellow needles, respectively, as minor products from this method. Both crystals refined in monoclinic space group *P2₁/n* in low crystalline yield. The Ln1 site (within the macrocycle) was fully occupied and bound by six pyridyl and imine nitrogen atoms. The structure also showed evidence for Ln–O bonding interactions from the three hemiacetate oxygen atoms. These nitrogen and oxygen atoms are arranged around the pocketed Ln1 cation in a pseudotricapped trigonal prism. The capping Ln2 site sits above the macrocycle pocket. This Ln2 cation is bound by three oxygen atoms from the hemiacetate, six oxygen atoms from nitrate ligands, and one oxygen atom from a coordinated MeOH. These 10 oxygen atoms create a distorted bicapped square antiprism around Ln2 (Figure 1).

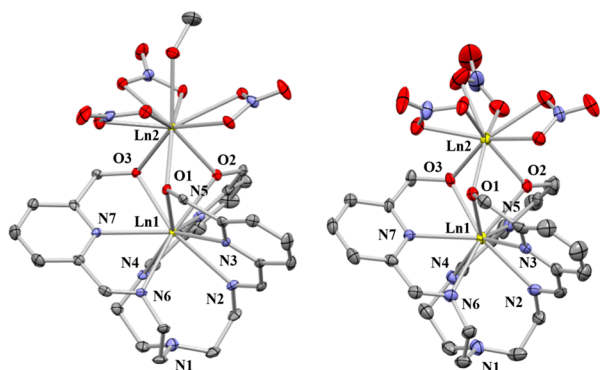


Figure 1. Molecular structure of Ln₂TPT^{OX}(MeOH) (left; Ln = Ce–Sm) and Ln₂TPT^{OX} (right; Ln = Eu–Lu) drawn with 50% probability ellipsoids. Hydrogen atoms, pendant X groups (OX = OMe, OMeOEt, OBz), and the lattice solvent are omitted for clarity.

Examination of the mother liquor revealed formation of the trinitrate [H₃Tren][NO₃]₃ biproduct. A scheme accounting for the mass balance of the reaction is provided (Scheme S1).

The crystals obtained from analogous reactions with neodymium and samarium nitrates were more complicated than that observed for the larger cerium and praseodymium cations. Here, two crystal morphologies were observed in a roughly 2:1 ratio. The majority products were yellow plates identified as Nd₂TPT^{OMe} and Sm₂TPT^{OMe} that refined in the orthorhombic space group *P222*, which were separated from orange blocks of NdTPT and SmTPT, analogous structures to

the reported compounds.²⁴ Nd₂TPT^{OMe} and Sm₂TPT^{OMe} were isostructural to the solid-state structures of Ce₂TPT^{OMe} and Pr₂TPT^{OMe}.

Progression along the lanthanide series to the smaller cations (Eu–Lu) resulted in the formation of Ln₂TPT^{OMe} (Ln = Eu–Lu), which were isolated as yellow crystalline needles in high yield. Single-crystal X-ray diffraction data obtained of these crystals were modeled in the *P222* space group. The terminal metal, Ln2, is nine-coordinate, owing to the absence of a coordinated MeOH. For the whole series, the Ln1–Ln2 distance decreases linearly with decreasing ionic radius, with the largest separation of 3.689(1) Å for cerium and the smallest separation of 3.347(1) Å for lutetium (Table 1).

Table 1. Metrical Comparisons of Averaged Ln₂TPT^{OMe} (Ln = Ce–Sm) and Ln₂TPT^{OMe} (Ln = Eu–Lu) Complexes^a

Ln1	Ln–N _{Tren} (Å) ^a	Ln–N _{pyr} (Å) ^a	Ln1–Ln2 (Å)	Ln1–O–Ln2 (deg)
Ce	2.738(2)	2.650(2)	3.689(1)	97.89(6)
Pr	2.721(3)	2.621(3)	3.656(1)	97.59(8)
Nd	2.677(4)	2.581(4)	3.587(2)	96.66(9)
Sm	2.657(4)	2.560(4)	3.548(1)	96.64(2)
Eu	2.632(5)	2.547(5)	3.506(1)	96.04(1)
Gd	2.616(4)	2.540(4)	3.487(1)	95.80(1)
Tb	2.606(5)	2.524(5)	3.457(1)	95.75(5)
Dy	2.602(5)	2.504(5)	3.447(1)	95.61(1)
Ho	2.599(4)	2.461(4)	3.437(1)	95.30(1)
Er	2.579(8)	2.465(8)	3.394(2)	95.23(2)
Tm	2.567(4)	2.476(4)	3.383(1)	95.26(1)
Yb	2.564(7)	2.419(7)	3.363(1)	94.90(2)
Lu	2.554(6)	2.458(6)	3.347(1)	94.70(2)

^aN_{Tren} = N2, N4, N6; N_{pyr} = N3, N5, N7.

Several other structural metrics for the complexes change proportionally to the ionic radius of the metal. The pocket size of the ligand adjusts to the size of the lanthanide, and the Ln1–N1 distance (N1 = tertiary nitrogen of Tren) and C–N1–C angle increase with decreasing ionic radius (Figure 2). The smaller the cation, the more closely to the metal center the pyridyl nitrogen atom coordinates, causing an increase to the pyramidalization angle of N1. The twist angles of the ligand are also affected by the size of the metal ion; a linear trend in

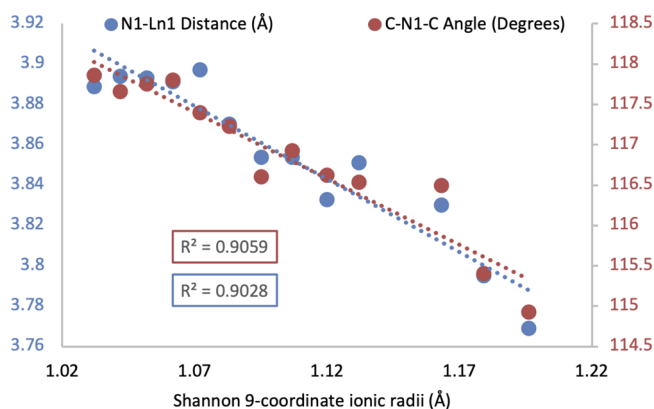


Figure 2. (Blue) Plot of the N1–Ln1 distance (Å) for Ln₂TPT^{OMe} (Ln = Ce–Sm) and Ln₂TPT^{OMe} (Ln = Eu–Lu). (Red) Plot of the average C–N1–C angle (nitrogen pyramidalization) for Ln₂TPT^{OMe} (Ln = Ce–Sm) and Ln₂TPT^{OMe} (Ln = Eu–Lu).

the twist angle is observed during the comparison of the planes formed from the imine nitrogen atoms, the pyridyl nitrogen atoms, and the hemiacetate bridging oxygen atoms as the metal is changed (Table S1 and Figures S32–S35).

The ^1H and ^{13}C NMR spectra of $\text{Lu}_2\text{TPT}^{\text{OMe}}$ in deuterated dimethyl sulfoxide ($\text{DMSO}-d_6$) show unexpected but reproducible minor peaks that suggest the formation of isomeric complexes. Perhaps these peaks result from DMSO coordinating the $\text{Lu}_2\text{TPT}^{\text{OMe}}$ complex, but we cannot rule out the possibility of $\text{Lu}_2\text{TPT}^{\text{OMe}}$ decomposition products or dissociation of the terminal metal. Importantly, CHN analysis confirms the compositional purity of the bulk sample. We attempted crystallization of the complex from DMSO, and the resulting structure was identical with the structure obtained from MeOH and had no sign of DMSO coordination. The sample showed signs of decomposition when analyzed by ^1H NMR spectroscopy in deuterated water (D_2O). We suspected that the water content of DMSO contributed to the extra peaks in the ^1H NMR spectrum. The extra peaks, however, were reproducible in different batches of DMSO that had been dried and degassed.

To probe the source of unexpected resonances, we performed the synthesis of $\text{Lu}_2\text{TPT}^{\text{OMe}}$ in $\text{MeOH}-d_4$ to incorporate the label into the hemiacetal group and to acquire NMR data in this solvent and forego the possibility of decomposition in DMSO. The poor solubility of the complex in MeOH did not improve the results from ^1H NMR analysis; the complex almost quantitatively precipitated from solution, and analysis of the mother liquor revealed only peaks for $[\text{H}_3\text{Tren}][\text{NO}_3]_3$ (Figure S21). We were still able to confirm the origin of the methoxy groups of the ligand. Analysis of the precipitated product in $\text{DMSO}-d_6$ showed the expected disappearance of the $-\text{OMe}$ singlet at 3.57 ppm in the ^1H NMR spectrum and 53.55 ppm in the ^{13}C NMR spectrum, with a new multiplet centered at 53.39 ppm in the ^{13}C NMR spectrum. The small peaks were present in the same ratio as that in previous spectra.

We next extended the reactivity of alcoholic cleavage to probe other primary alcohols, using 2-methoxyethanol and benzyl alcohol as solvents. These experiments were conducted with diamagnetic lutetium, which facilitated characterization by NMR spectroscopy. This resulted in the formation of hemiacetal-bridged species with 2-methoxyethyl or benzyl groups in place of the methyl group of the hemiacetate fragment (Figure 3). $\text{Lu}_2\text{TPT}^{\text{OMeOEt}}$ and $\text{Lu}_2\text{TPT}^{\text{OBz}}$ were refined in the monoclinic space group $P2_1/n$. $\text{Lu}_2\text{TPT}^{\text{OBz}}$ crystallized with low crystalline yield as pale-yellow needles

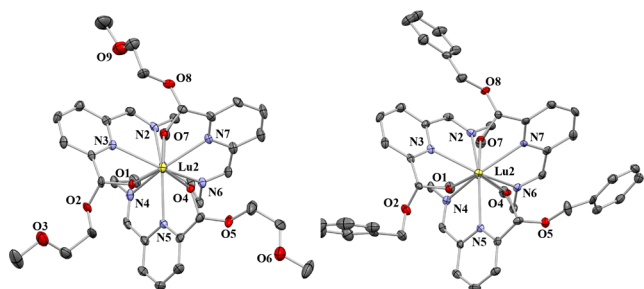


Figure 3. Molecular structures of $\text{Lu}_2\text{TPT}^{\text{OMeOEt}}$ (left) and $\text{Lu}_2\text{TPT}^{\text{OBz}}$ (right) drawn at 50% probability, with hydrogen atoms, nitrate groups, disorder, and solvent molecules omitted for clarity. Viewed along the Lu1–Lu2 axis.

physically separated from an amorphous powder and was obtained as an impure mixture. A comparison of the solid-state metrics shows that $\text{Lu}_2\text{TPT}^{\text{OBz}}$ has significantly shorter Lu1–Lu2 and Lu1– N_{Tren} ($\text{N}_{\text{Tren}} = \text{N}2, \text{N}4, \text{N}6$; Figure 1) bond distances than what is observed for $\text{Lu}_2\text{TPT}^{\text{OMe}}$ (Table 2). In

Table 2. Metrical Comparisons of Averaged $\text{Lu}_2\text{TPT}^{\text{X}}$ ($\text{X} = \text{OMe}, \text{OMeOEt}, \text{OBz}$) Complexes

	TPT^{OMe}	$\text{TPT}^{\text{OMeOEt}}$	TPT^{OBz}
Ln– N_{Tren} (Å)	2.554(6)	2.552(4)	2.533(3)
Ln– N_{pyr} (Å)	2.458(6)	2.467(4)	2.467(3)
Ln1–Ln2 (Å)	3.347(1)	3.340(1)	3.327(1)
Ln1–O–Ln2 (deg)	94.7(2)	94.2(1)	94.0(1)
N1–Ln1 (Å)	3.889(7)	3.870(4)	3.887(4)
C–N1–C (deg)	117.8(7)	117.6(4)	118.3(4)

terms of size correlation, the steric demands of the benzyl group distort the complex metrics from those observed with $\text{Lu}_2\text{TPT}^{\text{OMe}}$ to a greater degree than the methoxyethanol group. Other alcohols such as phenol, isopropyl alcohol, and *tert*-butanol were unsuccessfully attempted. ^1H NMR analysis of $\text{Lu}_2\text{TPT}^{\text{OMeOEt}}$ reveals a much cleaner spectrum than $\text{Lu}_2\text{TPT}^{\text{OMe}}$, suggesting either a lower ratio of isomer formation or enhanced stability of the complex, both likely arising from the greater steric influence of the larger alcohol. All expected resonances for the complex were observed alongside minor signals, peaks far less intense than those observed in $\text{Lu}_2\text{TPT}^{\text{OMe}}$.

Single-crystal UV/vis/near-IR spectra from $\text{Ln}_2\text{TPT}^{\text{OMe}}$ complexes reveal intense, broad absorption peaks with λ_{max} near 400 nm (see the Supporting Information). Weaker peaks at lower energy were resolved from this intense absorption band between 450 and 1100 nm. These features were attributed to Laporte-forbidden $4f \rightarrow 4f$ transitions and were most prominent for Ln = Nd, Dy, and Ho. Excitation at 420 nm shows several intense features observed only for $\text{Eu}_2\text{TPT}^{\text{OMe}}$, and fluorescence peaks were identified at 593, 617, and 698 nm (Figure S11). Solid-state IR spectra were similar for all complexes, with bands at 1600 and 1590 cm^{-1} , frequencies attributed to the imine stretches of the complexes. SQUID data were obtained for $\text{Gd}_2\text{TPT}^{\text{OMe}}$ and $\text{Dy}_2\text{TPT}^{\text{OMe}}$ to probe variable-temperature magnetic behavior (Figures S29–S31). While helicate complexes have shown unusual magnetic characteristics at lower temperatures,²⁶ prior work by Winpenny et al.²⁷ on related oxo-bridged bimetallic complexes has shown only minor coupling between the metal centers. Consistent with this, $\text{Gd}_2\text{TPT}^{\text{OMe}}$ and $\text{Dy}_2\text{TPT}^{\text{OMe}}$ displayed magnetic behavior in agreement with little interaction between the metal cations. Average respective moments of 8.3 and 11.08 μ_{B} (300 K) were obtained for gadolinium and dysprosium, values near the accepted moments of the free metal cations (8.0 μ_{B} for gadolinium and 10.6 μ_{B} for dysprosium).^{28–30}

The methodology presented on the synthesis, isolation, and characterization of bimetallic $\text{Ln}_2\text{TPT}^{\text{OMe}}$ complexes contributes to the field of 4f-element chelation chemistry. Expanding the landscape of lanthanide self-assembly reactions to include a new form of reactivity with TPT ligands allows for further studies of a series of related bimetallic lanthanide compounds. Our work involved the formation of half-cage complexes via imine cleavage to form a lanthanide-bound, bridging hemiacetate functionality. Although the generality of this reaction

type has yet to be fully explored, this methodology has potential value in terms of accessing additional high-nuclearity f-element complexes, with future potential supporting innovation within the subfields of molecular magnetism, separations, and radiopharmaceuticals. We are particularly excited about the opportunities this type of reactivity may have for 5f elements, and we are continuing to pursue additional self-assembly reactions with lanthanide and actinide cations.

■ ASSOCIATED CONTENT

SI Supporting Information

The Supporting Information is available free of charge at <https://pubs.acs.org/doi/10.1021/acs.inorgchem.0c00775>.

Experimental details, photographs of compounds, characterization spectra, magnetometry, selected bond distances, and crystallographic tables for all complexes (PDF)

Accession Codes

CCDC 1948574–1948588 contain the supplementary crystallographic data for this paper. These data can be obtained free of charge via www.ccdc.cam.ac.uk/data_request/cif, or by emailing data_request@ccdc.cam.ac.uk, or by contacting The Cambridge Crystallographic Data Centre, 12 Union Road, Cambridge CB2 1EZ, UK; fax: +44 1223 336033.

■ AUTHOR INFORMATION

Corresponding Author

Aaron M. Tondreau – Los Alamos National Laboratory (LANL), Los Alamos, New Mexico 87544, United States; orcid.org/0000-0003-0440-5497; Email: tondreau_a@lanl.gov

Authors

Bonnie E. Klamm – Los Alamos National Laboratory (LANL), Los Alamos, New Mexico 87544, United States; Department of Chemistry and Biochemistry, Florida State University, Tallahassee, Florida 32306, United States; orcid.org/0000-0002-1168-0932

Thomas E. Albrecht-Schmitt – Department of Chemistry and Biochemistry, Florida State University, Tallahassee, Florida 32306, United States; orcid.org/0000-0002-2989-3311

Ryan E. Baumbach – National High Magnetic Field Laboratory, Tallahassee, Florida 32310, United States

Brennan S. Billow – Los Alamos National Laboratory (LANL), Los Alamos, New Mexico 87544, United States; orcid.org/0000-0002-7560-9369

Frankie D. White – Los Alamos National Laboratory (LANL), Los Alamos, New Mexico 87544, United States

Stosh A. Kozimor – Los Alamos National Laboratory (LANL), Los Alamos, New Mexico 87544, United States; orcid.org/0000-0001-7387-0507

Brian L. Scott – Los Alamos National Laboratory (LANL), Los Alamos, New Mexico 87544, United States

Complete contact information is available at:

<https://pubs.acs.org/doi/10.1021/acs.inorgchem.0c00775>

Author Contributions

‡These authors contributed equally. The manuscript was written through contributions of all authors. All authors have given approval to the final version of the manuscript.

Notes

The authors declare no competing financial interest.

■ ACKNOWLEDGMENTS

This work was conceived and executed at LANL. Funding at LANL was provided by the Director, Office of Science, Office of Basic Energy Sciences, Division of Chemical Sciences, Geosciences, and Biosciences, Heavy Element Chemistry Program of the U.S. Department of Energy (DOE), the Laboratory Directed Research and Development program of LANL under Projects 20180128ER and 2019057ECR, the Seaborg Institute, and a Summer Research Fellowship awarded to B.E.K. B.E.K. and T.E.A.-S. thank the Chemical Sciences, Geosciences, and Biosciences Division of the Office of Basic Energy Sciences of the U.S. DOE for supporting the research as part of the Center for Actinide Science and Technology funded by the U.S. DOE, Office of Science, Office of Basic Energy Sciences, under Award DE-SC0016568. A portion of this work was performed at the National High Magnetic Field Laboratory, which is supported by National Science Foundation Cooperative Agreement DMR-1644779 and the State of Florida.

■ REFERENCES

- (1) Sato, T.; Sakai, K.; Tsubomura, T. Conformational Change of a Macrobicyclic Complex. Structure of Free Ligand and Interactions with DMSO. *Chem. Lett.* **1993**, *22* (5), 859–862.
- (2) Bunzli, J. Lanthanide Luminescence for Biomedical Analyses and Imaging. *Chem. Rev.* **2010**, *110*, 2729–2755.
- (3) Heffern, M.; Matosziuk, L.; Meade, T. Lanthanide Probes for Bioresponsive Imaging. *Chem. Rev.* **2014**, *114* (8), 4496–4539.
- (4) Blanusa, M.; Varnai, V.; Piasek, M.; Kostial, K. Chelators as Antidotes of Metal Toxicity: Therapeutic and Experimental Aspects. *Curr. Med. Chem.* **2005**, *12* (23), 2771–2794.
- (5) Xue, X.; Wang, F.; Liu, X. Emerging Functional Nanomaterials for Therapeutics. *J. Mater. Chem.* **2011**, *21*, 13107–13127.
- (6) Kronholm, B.; Anderson, C. G.; Taylor, P. R. A Primer on Hydrometallurgical Rare Earth Separations. *JOM* **2013**, *65* (10), 1321–1326.
- (7) Paulenova, A. Physical and Chemical Properties of Actinides in Nuclear Fuel Reprocessing. In *Advanced Separation Techniques for Nuclear Fuel Reprocessing and Radioactive Waste Treatment*; Woodhead Publishing Series in Energy 2; Nash, K. L., Lumetta, G. J., Eds.; Woodhead Publishing, 2011; pp 23–57; DOI: 10.1533/9780857092274.1.23.
- (8) Tranter, T. J. Solid-Phase Extraction Technology for Actinide and Lanthanide Separations in Nuclear Fuel Reprocessing. In *Advanced Separation Techniques for Nuclear Fuel Reprocessing and Radioactive Waste Treatment*; Woodhead Publishing Series in Energy 13; Nash, K. L., Lumetta, G. J., Eds.; Woodhead Publishing, 2011; pp 377–413; DOI: 10.1533/9780857092274.3.377.
- (9) Hill, C. Development of Highly Selective Compounds for Solvent Extraction Processes: Partitioning and Transmutation of Long-Lived Radionuclides from Spent Nuclear Fuels. In *Advanced Separation Techniques for Nuclear Fuel Reprocessing and Radioactive Waste Treatment*; Woodhead Publishing Series in Energy 11; Nash, K. L., Lumetta, G. J., Eds.; Woodhead Publishing, 2011; pp 311–362; DOI: 10.1533/9780857092274.3.311.
- (10) Veliscek-Carolan, J. Separation of Actinides from Spent Nuclear Fuel: A Review. *J. Hazard. Mater.* **2016**, *318*, 266–281.
- (11) Pearson, R. Hard and Soft Acids and Bases. *J. Am. Chem. Soc.* **1963**, *85* (22), 3533–3539.
- (12) Aravena, D.; Atanasov, M.; Neese, F. Periodic Trends in Lanthanide Compounds through the Eyes of Multireference Ab Initio Theory. *Inorg. Chem.* **2016**, *55* (9), 4457–4469.
- (13) Cotton, S. A.; Raithby, P. R. Systematics and Surprises in Lanthanide Coordination Chemistry. *Coord. Chem. Rev.* **2017**, *340*, 220–231.

(14) Boland, K. S.; Hobart, D. E.; Kozimor, S. A.; MacInnes, M. M.; Scott, B. L. The Coordination Chemistry of Trivalent Lanthanides (Ce, Nd, Sm, Eu, Gd, Dy, Yb) with Diphenyldithiophosphinate Anions. *Polyhedron* **2014**, *67*, 540–548.

(15) Hamilton, A. D. Crown Ethers and Cryptands. *Compr. Heterocycl. Chem.* **1984**, 731–761.

(16) Suresh Kumar, D.; Alexander, V. Synthesis of Lanthanide(III) Complexes of Chloro- and Bromo Substituted 18-Membered Tetraaza Macrocycles. *Polyhedron* **1999**, *18* (11), 1561–1568.

(17) Radecka-Paryzek, W.; Patroniak-Krzyminiewska, V.; Litkowska, H. The Template Synthesis and Characterization of the Yttrium and Lanthanide Complexes of New 19-Membered Pentadentate Azaoxa Macrocyclic. *Polyhedron* **1998**, *17* (9), 1477–1480.

(18) Radecka-Paryzek, W.; Patroniak, V.; Lisowski, J. Metal Complexes of Polyaza and Polyoxaaza Schiff Base Macrocycles. *Coord. Chem. Rev.* **2005**, *249* (21–22), 2156–2175.

(19) Manseki, K.; Sakiyama, H.; Sakamoto, M.; Nishida, Y.; Aono, H.; Sadaoka, Y.; Ohba, M.; Okawa, H. A New Type Copper(II)-Gadolinium(III) Complex of Phenol-Based Side-Off Type Dinucleating Ligand Containing Fully Saturated Amino Nitrogens as Coordinating Atoms. *Synth. React. Inorg. Met.-Org. Chem.* **2001**, *31* (8), 1443–1451.

(20) Brianese, N.; Casellato, U.; Tamburini, S.; Tomasin, P.; Vigato, P. A. Functionalized Acyclic Schiff Bases and Related Complexes with D- and f-Metal Ions. *Inorg. Chim. Acta* **1998**, *272* (1–2), 235–251.

(21) Echenique-Erandonia, E.; Zabala-Lekuona, A.; Cepeda, J.; Rodríguez-Diéguez, A.; Seco, J. M.; Oyarzabal, I.; Colacio, E. Effect of the Change of the Ancillary Carboxylate Bridging Ligand on the SMM and Luminescence Properties of a Series of Carboxylate-Diphenoxido Triply Bridged Dinuclear ZnLn and Tetranuclear Zn₂Ln₂ Complexes (Ln = Dy, Er). *Dalt. Trans.* **2019**, *48* (1), 190–201.

(22) Hu, X.; Qiu, L.; Sun, W.; Ng, S. [1,4,12,15,18,26,31,39,42,43,44-Undeca-aza-penta-cyclo-[13.13.13.16,10.120,24.133,37]Tetra-tetra-conta-4,6,8,10-(44),11,18,20,22,24(43),25,31,33,35,37(42),38-Penta-deca-ene-K9N4, N11, N18, N26, N31, N39, N42, N43, N44]Gadolinium(III) Trichloride Trihydrate. *Acta Crystallogr., Sect. E: Struct. Rep. Online* **2006**, *62* (12), m3351–m3353.

(23) Hu, X.; Li, Y.; Luo, Q. Characterization and Crystal Structure of Lanthanide Cryptates of a Ligand Derived from 2,6-Diformyl Pyridine. *Polyhedron* **2004**, *23* (1), 49–53.

(24) Hu, X.; Li, Y.; Luo, Q. Synthesis and Crystal Structure of a New Neodymium Cryptate of a Ligand Derived from 2,6-Diformylpyridine. *J. Coord. Chem.* **2003**, *56* (15), 1277.

(25) Xuelei, H.; Li, Q.; Zhong, C.; Qimao, H.; Zhiquan, P. Synthesis of Alkaline Earth and Lanthanide Cryptates with Pyridine-Based Group. *J. Rare Earths* **2007**, *25* (6), 674–678.

(26) Martin, N.; Bünzli, J.-C. G.; McKee, V.; Piguet, C.; Hopfgartner, G. Self-Assembled Dinuclear Lanthanide Helicates: Substantial Luminescence Enhancement upon Replacing Terminal Benzimidazole Groups by Carboxamide Binding Units. *Inorg. Chem.* **1998**, *37* (3), 577–589.

(27) Giansiracusa, M. J.; Moreno-Pineda, E.; Hussain, R.; Marx, R.; Martínez Prada, M.; Neugebauer, P.; Al-Badran, S.; Collison, D.; Tuna, F.; van Slageren, J.; Carretta, S.; Guidi, T.; McInnes, E. J. L.; Winpenny, R. E. P.; Chilton, N. F. Measurement of Magnetic Exchange in Asymmetric Lanthanide Dimetallics: Toward a Transferable Theoretical Framework. *J. Am. Chem. Soc.* **2018**, *140* (7), 2504–2513.

(28) Bünzli, J.-C. G.; André, N.; Elhabiri, M.; Muller, G.; Piguet, C. Trivalent Lanthanide Ions: Versatile Coordination Centers with Unique Spectroscopic and Magnetic Properties. *J. Alloys Compd.* **2000**, *303–304*, 66–74.

(29) Orchard, A. F. *Magnetochemistry*; Oxford University Press, 2003.

(30) Carlin, R. L. Rare Earths or Lanthanides. *Magnetochemistry*; Springer: Berlin, 1986; pp 237–261.